Nuclear Engineering and Design 362 (2020) 110579

Contents lists available at ScienceDirect

Nuclear Engineering and Design

journal homepage: www.elsevier.com/locate/nucengdes

# Plugging criteria and stress determination for high-pressure feedwater heater tubes with local wall-thinning

Hong Bo Dinh[a], Kee Bong Yoon[b,*]

[a] Hanoi University of Science and Technology, No. 1, Dai Co Viet road, Hai Ba Trung, Hanoi, Viet Nam
[b] Department of Mechanical Engineering, Chung Ang University, 84, Heukseok-ro, Dongjak, Seoul 06974, Republic of Korea

ARTICLE INFO

*Keywords:*
Finite element analysis
Feedwater heater tube
Local wall-thinning defect
Plugging criteria
Regression method

ABSTRACT

Tubes with local wall-thinning defects are often found in the heat exchangers of high-pressure feedwater heaters in thermal power plants. When serious damage is found in a tube, the tube is taken out of service by plugging it to prevent rupturing at the location of the local wall-thinning defect. This paper introduces a theoretical and numerical analysis of the stresses found in feedwater heater tubes with local wall-thinning defects under pressure and thermal loads. The effect of the dimensions of this defect on these stresses is also studied.

Using finite element analysis and regression, analytic equations for the hoop and axial stress on the inner surface of a tube with a local wall-thinning defect are proposed. The plugging criteria for a tube with this form of defect are also determined using von Mises stress theory. It is found that maximum stress occurs on the inner surface of the tube. The radial stress on the inner surface does not depend on the $c/t$ and $c/b$ ratio; rather, depth ($c$) is the main factor influencing overall stress (i.e., hoop, axial, and von Mises stress), with hoop and axial stress increasing as the depth increases. The longitudinal length ($2b$) also has an effect on hoop and axial stress. When the depth increases ($c/t = 0.3$–$0.5$), the effect of $b$ is more prominent. The procedure used in this study is independent of the material properties and operating conditions, so it can be applied to other tube materials under various operating conditions in high-pressure feedwater heaters.

## 1. Introduction

A feedwater heater is a power plant component used to pre-heat water delivered to a steam-generating boiler. Pre-heating the feedwater improves the thermodynamic efficiency of the plant and significantly reduces fuel consumption. Shell-tube feedwater heaters are one of the most common types of heat exchanger and are particularly well-suited to high-pressure industrial applications. There are several variations of the shell and tube design. The tubes may be straight or bent into a U-shape which are called U-tubes.

In any heater, many tubes are installed for the purpose of heat exchange and are maintained based on periodic inspections for safe operation. The service records of many shell-and-tube heat-exchangers demonstrate that the tubes are particularly susceptible to local wall-thinning defects, mostly due to the combined actions of corrosion, erosion, pitting, fretting wear, cracks (Tun et al., 2016; Yoon et al., 2003), and various types of other wear (Moreira Junior et al., 2015; Wang et al., 2013; Zhang et al., 2016). Tubes are subject to local wall-thinning from either the inside or outside. When serious damage is found in a tube, the tube is taken out of service by plugging it.

Previous studies have focused on the burst pressure in tubes with geometric eccentricities (Chen et al., 2015a,b, 2016) and in steam generator tubes with multiple axial surface cracks (Kim et al., 2019). The plugging criteria for high-pressure feedwater heater tubes with outer thinning (either uniform or eccentric thinning) in accordance with pressure and thermal loading have also been analyzed (Dinh et al., 2018). It has also been found that tubes with local wall-thinning defects are a common occurrence in the heat exchangers of feedwater heaters in thermal power plants. In this respect, an experimental and numerical analysis of the plastic limit loads in Inconel 690 steam generator tubes with local wall-thinning defects has previously been conducted (Hui and Li, 2010), but the plugging criteria for these defective tubes have not been analyzed. There has also been little research on the effect of the dimensions of local wall-thinning defects within feedwater heater tubes on associated stress.

The aim of the research is to determine the plugging criteria and stresses present within feedwater heater tubes with local wall-thinning defects using finite element and regression analysis. The effect of the dimensions (i.e., the $c/t$ and $c/b$ ratios) of the local wall-thinning defect on the stresses within the tube is also analyzed. Using regression,

* Corresponding author.
*E-mail address:* kbyoon@cau.ac.kr (K.B. Yoon).

https://doi.org/10.1016/j.nucengdes.2020.110579
Received 16 June 2019; Received in revised form 16 February 2020; Accepted 17 February 2020
Available online 04 March 2020

**Nomenclature**

| | | | |
|---|---|---|---|
| $T_o$ | Temperature of the steam | $\sigma_{z,p}$ | Axial stress due to pressure loading |
| $T_i$ | Temperature of the feedwater | $\sigma_{r,p}$ | Radial stress due to pressure loading |
| $T_o$* | Temperature on the outer surface of the tube | $\sigma_{\theta,th}$ | Hoop stress due to thermal loading |
| $T_i$* | Temperature on the inner surface of the tube | $\sigma_{z,th}$ | Axial stress due to thermal loading |
| $P_o$ | External pressure | $\sigma_{r,th}$ | Radial stress due to thermal loading |
| $P_i$ | Internal pressure | $\sigma_\theta$ | Hoop stress due to combined loadings |
| $D$ | Outer diameter of the tube | $\sigma_z$ | Axial stress due to combined loadings |
| $r$ | Radius of the tube | $\sigma_r$ | Radial stress due to combined loadings |
| $r_o$ | Outer radius of the tube | $\sigma_{allow}$ | Maximum allowable stress |
| $r_i$ | Inner radius of the tube | $\sigma_{proof}$ | Proof stress |
| $t$ | Wall thickness | $\sigma_{Von}$ | Von Mises stress |
| $\sigma_{\theta,p}$ | Hoop stress due to pressure loading | $n$ | The safety factor |
| | | $c$ | The depth of the local wall-thinning defect |
| | | $2b$ | The length of the local wall-thinning defect |

analytic equations for hoop and axial stress on the inner surface of a tube with a local wall-thinning defect are proposed. Comparing these equations with the results of finite element analysis verifies this approach to analyzing defective tubes.

## 2. Numerical model for a tube with a local wall-thinning defect

### 2.1. Problem description

A feedwater heater for a 500-MW fossil fuel power plant was considered in this study. This heater contained U-tube heat exchangers to transfer heat from high-temperature steam outside of the tubes to water inside the tubes through the tube wall. This study focused on the straight section of a U-tube in the de-superheating zone, which is the location most susceptible to failure via the thinning of the tube wall due to it having the highest temperature difference between the inner and outer surfaces of the tube and being exposed to high-velocity vertical flows of incoming steam.

The straight section of a U-tube in the de-superheating zone was thus selected as the model for this study (Fig. 1). The temperature of the steam outside the tube $T_o$ was set at 416.5 °C, with an external pressure $P_o$ of 1.89 MPa, while the temperature of the feedwater inside the tube $T_i$ was set at 204.5 °C, with an internal pressure $P_i$ of 35.89 MPa. Axial force $R$ due to the thrust of the pressure towards the end-cap was applied at one of the ends of the straight section. The tube thickness and outer diameter were 2.2 mm and 15.9 mm, respectively. A typical form of local wall-thinning defect for U-tubes was considered in this paper (Fig. 2).

### 2.2. Finite element analysis for a tube with a local wall-thinning defect

#### 2.2.1. Finite element modeling and analysis approach

Finite element analysis (FEA) was employed using ABAQUS (version 6.14) to determine the mechanical and thermal stresses on the model U-tube. A three-dimensional model of the tube was constructed. Elastic behavior was considered in this study, and the analysis was conducted based on small displacements. A half model of the structure of a 300 mm length of a feedwater heater tube was used to take advantage

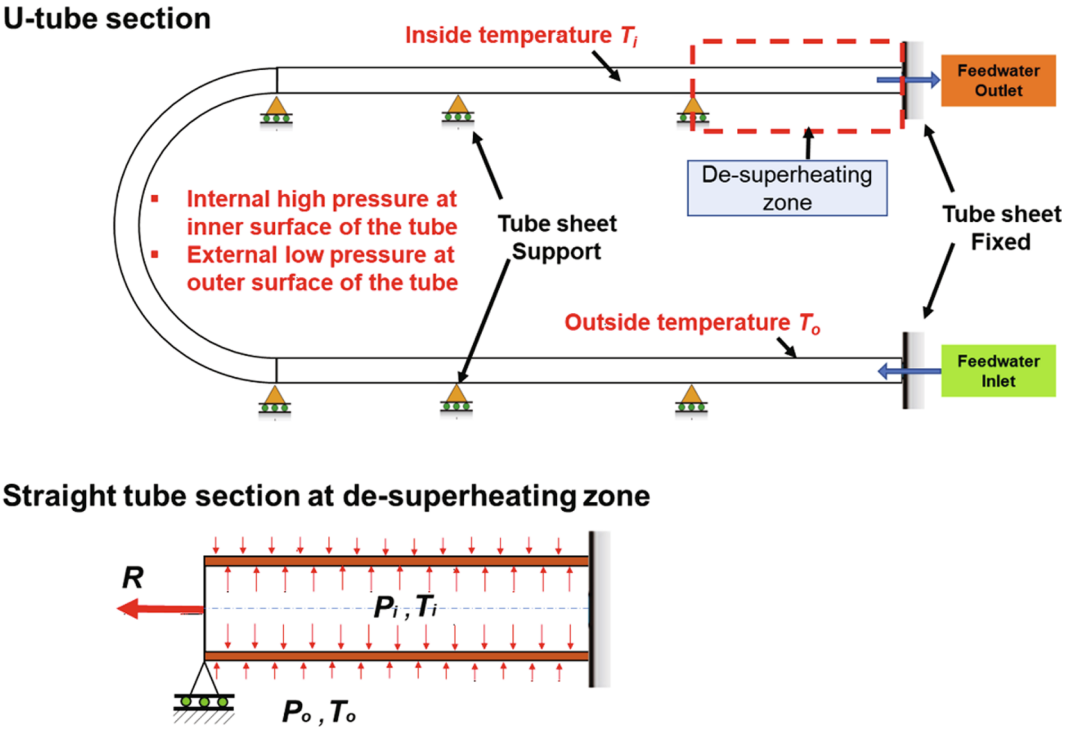


**Fig. 1.** Modeling of the straight section of a U-tube in the de-superheating zone of a feedwater heater.

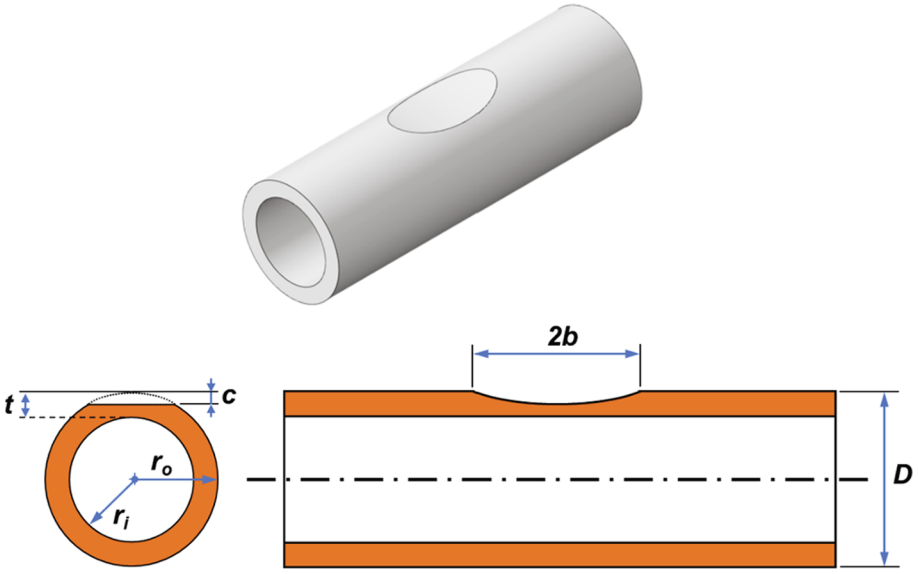


**Fig. 2.** Modeling of a tube with a local wall-thinning defect.

of symmetry, and the internal pressure, external pressure, and temperature gradient were analyzed. An axial uniform load was added to one end of the tube to represent the thrust of pressure, while the other end of the tube was modeled using symmetry plane-*z*. Symmetric restrictions were applied to the symmetric boundary plane-*x*. Fig. 3 presents further details regarding the loads, boundary conditions, and meshing of the model tube with a local wall-thinning defect. Mesh independence was confirmed before using the model with 238,111 elements to make sure the convergence of the results.

The tubes for the feedwater heater were fabricated from seamless stainless SA-213 Grade TP304N material. The mechanical properties of this material can be found in the ASME Code, Section II, Part D (ASME Boiler and Pressure Vessel Code, Section II, 2013). To calculate the heat transfer from the steam through the tube wall to the feedwater, the convective heat transfer coefficient was considered for both the inner and outer surfaces of the tube. Other parameters such as Young's modulus ($E$), thermal conductivity ($k$), the thermal expansion coefficient ($\alpha$), yield strength ($\sigma_{YS}$), and ultimate tensile strength ($\sigma_{UTS}$) are presented in Table 1, as determined based on the average of the inner and outer temperatures of the tube (235 °C).

**Table 1**
Material properties of SA-213 Grade TP304N at 235 °C.

| Material properties | SA-213 Grade TP304N |
|---|---|
| Young's modulus (GPa) | 175 |
| Poisson's ratio | 0.31 |
| Density (kg/m$^3$) | 8100 |
| Thermal conductivity (W/m. °C) | 19.6 |
| Thermal expansion coefficient (°C$^{-1}$) | 17.8 × 10$^{-6}$ |
| Heat transfer coefficient on the outer surface (W/m$^2$. °C) | 1,500 |
| Heat transfer coefficient on the inner surface (W/m$^2$. °C) | 23,400 |
| Yield strength (MPa) | 149 (at 235 °C) |
| Ultimate tensile strength (MPa) | 497 (at 235 °C) |

*2.2.2. Effect of the defect dimensions on stresses within the tube*

Using FEA, the stresses in the local wall-thinning zone are assessed for various values of $c$ (0.22, 0.44, 0.66, 0.88, 1.10 mm) and $b$ (0.44–11 mm), where $c$ and $b$ are the dimensions of the local wall-thinning defect defined in Fig. 2. In order to reduce models in the FEA,

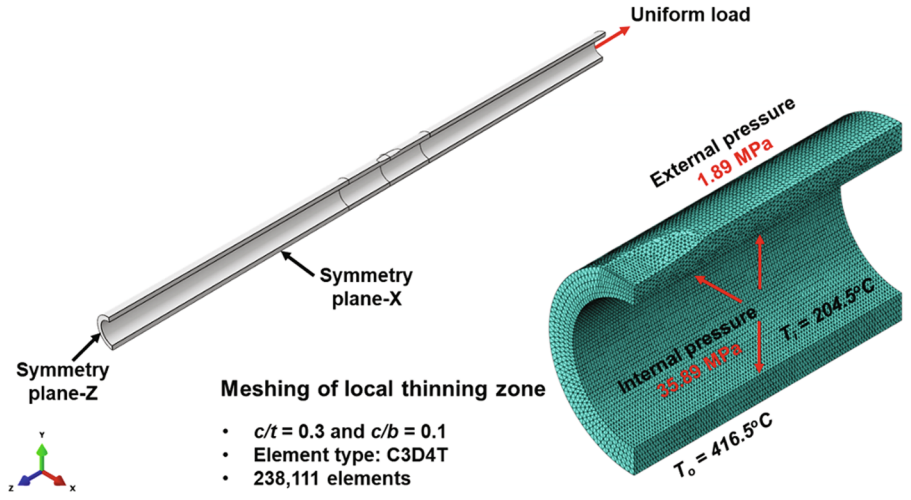


**Fig. 3.** Loads, boundary conditions, and meshing of a tube with a local wall-thinning defect.

the non-dimensional parameters $c/t$ and $c/b$ were employed, where $c/t$ is the ratio of the depth of the local wall-thinning defect to the wall thickness of the feedwater heater tube, and $c/b$ is the ratio of the depth of the local wall-thinning defect to the half-length along the axial direction of the defect.

In order to study the effect of the depth and length of the local wall-thinning defect on the overall stress, 25 variations of the FEA model are established based on different combinations of the $c/t$ (0.1, 0.2, 0.3, 0.4, 0.5) and $c/b$ (0.1, 0.2, 0.3, 0.4, 0.5) ratios. The FEA results for maximum von Mises stress are presented in Table 2, while those for hoop and axial stress are displayed in Fig. 4. For a local wall-thinning defect, it can be observed that

(1) Maximum stress is located on the inner surface of the tube. The radial stress on the inner surface does not depend on the $c/t$ and $c/b$ ratio and is approximately equal to the internal pressure (-35.89 MPa).
(2) The depth ($c$) of the defect is the main factor influencing hoop, axial, and von Mises stress, with hoop and axial stress increasing as the depth increases.
(3) The longitudinal length ($2b$) of the defect also affects the hoop and axial stress. When the depth increases ($c/t = 0.3^{-}0.5$), the effect of $b$ is most prominent, as shown in Fig. 4(a).

## 3. Suggested equations for hoop and axial stress on the inner surface

### 3.1. Analytic equations for stress in the absence of a local wall-thinning defect

The model tube was subject to both internal and external pressure. Hoop, axial, and radial stress as a function of the radius (Dinh et al., 2018) were given by Eqs. (1)–(3).

$$\sigma_{\theta,p} = \frac{P_i r_i^2 - P_o r_o^2}{r_o^2 - r_i^2} + \frac{(P_i - P_o) r_i^2 r_o^2}{(r_o^2 - r_i^2) r^2} \tag{1}$$

$$\sigma_{z,p} = \frac{P_i r_i^2 - P_o r_o^2}{r_o^2 - r_i^2} \tag{2}$$

$$\sigma_{r,p} = \frac{P_i r_i^2 - P_o r_o^2}{r_o^2 - r_i^2} - \frac{(P_i - P_o) r_i^2 r_o^2}{(r_o^2 - r_i^2) r^2} \tag{3}$$

Hoop, radial, and axial stress due to thermal loading was determined using Eqs. (4)–(6) (Poworoznek, 2008; Kanlıkama et al., 2013; Eslami et al., 2013). In these equations, $T_o$* and $T_i$* are the temperature on the outer surface and the inner surface of the tube, respectively.

$$\sigma_{\theta,th} = \frac{E\alpha(T_o^* - T_i^*)}{2\ln(r_o/r_i)} \left[ \frac{r_o^2}{r_o^2 - r_i^2} \left(1 + \frac{r_i^2}{r^2}\right) \ln\left(\frac{r_o}{r_i}\right) - \ln\left(\frac{r}{r_i}\right) - 1 \right] \tag{4}$$

$$\sigma_{r,th} = \frac{E\alpha(T_o^* - T_i^*)}{2\ln(r_o/r_i)} \left[ \frac{r_o^2}{r_o^2 - r_i^2} \left(1 - \frac{r_i^2}{r^2}\right) \ln\left(\frac{r_o}{r_i}\right) - \ln\left(\frac{r}{r_i}\right) \right] \tag{5}$$

$$\sigma_{z,th} = \frac{E\alpha}{1-\nu} \left( \frac{2\nu}{r_o^2 - r_i^2} \int_{r_i}^{r_o} Trdr - T \right) \quad \text{for plane strain} \tag{6}$$

where, $T$ is the temperature distribution inside the wall of the tube.

The three principal stresses were determined by superposing all of the stresses in the hoop, axial, and radial directions.

$$\sigma_\theta = \sigma_{\theta,p} + \sigma_{\theta,th} \tag{7}$$

$$\sigma_z = \sigma_{z,p} + \sigma_{z,th} \tag{8}$$

$$\sigma_r = \sigma_{r,p} + \sigma_{r,th} \tag{9}$$

### 3.2. Suggested equations for stresses in the presence of a local wall-thinning defect

#### 3.2.1. Hoop stress equation

To account for the presence of a local wall-thinning defect in the tube, the hoop stress equation for the inner surface must be modified:

$$\sigma_\theta = \left\{ \frac{(P_i r_i^2 - P_o r_o^2) + (P_i - P_o) r_o^2}{r_o^2 - r_i^2} + \frac{E\alpha(T_o^* - T_i^*)}{2\ln(r_o/r_i)} \left[ \frac{2r_o^2}{r_o^2 - r_i^2} \ln\left(\frac{r_o}{r_i}\right) - 1 \right] \right\} \times F_e\left(\frac{c}{t}, \frac{c}{b}\right) \tag{10}$$

where $F_e(c/t, c/b)$ is the hoop stress correction function for local thinning which depends on the parameters $c/t$ (0.1–0.5) and $c/b$ (0.1–0.5).

The expression for $F_e$ was obtained from the finite element solution for specific values of the $c/t$ and $c/b$ ratios.

$$F_e\left(\frac{c}{t}, \frac{c}{b}\right) = \frac{\sigma_{\theta\_FEM}}{\frac{(P_i r_i^2 - P_o r_o^2) + (P_i - P_o) r_o^2}{r_o^2 - r_i^2} + \frac{E\alpha(T_o^* - T_i^*)}{2\ln(r_o/r_i)} \left[ \frac{2r_o^2}{r_o^2 - r_i^2} \ln\left(\frac{r_o}{r_i}\right) - 1 \right]} \tag{11}$$

The interpolated function for $F_e$ was developed based on response surface modeling (RSM). RSM postulates a model of the form (Simpson and Mistree, 2001)

$y(x) = f(x) + \varepsilon$, (12) where, $y(x)$ is the unknown function of interest, $f(x)$ is the polynomial approximation of $\times$ , and $\varepsilon$ is random error. A second-order model was employed for optimization of the response $y$.

$$y = \beta_0 + \sum_{i=1}^{k} \beta_i x_i + \sum_{i=1}^{k} \beta_{ii} x_i^2 + \sum \sum_{i<j} \beta_{ij} x_i x_j + \varepsilon. \tag{13}$$

The parameters $\beta_o$, $\beta_i$, $\beta_{ii}$, and $\beta_{ij}$, of the polynomials in Eq. (13) were determined using least-squares regression, which minimizes the sum of the squares of the difference between the predicted and actual values. The coefficients of Eq. (13) were found using Eq. (14):

$$\beta = [X'X]^{-1}X'y, \tag{14}$$

where $X$ is the design matrix of sample data points, $X'$ is its transpose, and $y$ is a column vector that contains the values of the response at each sample point. The sample data and corresponding response values are summarized in Table 3. The second-order response surface model for the correction function $F_e$ was fit to the 25 sample points using ordinary least-squares regression. $F_e$ is given by Eq. (15):

$$F_e\left(\frac{c}{t}, \frac{c}{b}\right) = 1.1527 - 0.1573\left(\frac{c}{t}\right) + 0.0134\left(\frac{c}{b}\right) + 1.1586\left(\frac{c}{t}\right)^2 + 0.2657\left(\frac{c}{b}\right)^2 - 0.9400\left(\frac{c}{t}\right)\left(\frac{c}{b}\right) \tag{15}$$

#### 3.2.2. Axial stress equation

For general cases of a tube with a local wall-thinning defect under pressure and thermal loading, the following equation for axial stress on the inner surface was proposed:

**Table 2**
FEA results for maximum von Mises stress for different $c/t$ and $c/b$ ratios.

| $c/t$ ratio | $c/b$ ratio | | | | |
|---|---|---|---|---|---|
| | 0.1 | 0.2 | 0.3 | 0.4 | 0.5 |
| 0.1 | 190.4 | 193.5 | 193.1 | 193.1 | 194.5 |
| 0.2 | 190.6 | 191.4 | 191.5 | 195.1 | 192.1 |
| 0.3 | 194.5 | 194.9 | 193.1 | 193.1 | 193.6 |
| 0.4 | 201.0 | 194.5 | 192.9 | 192.4 | 192.8 |
| 0.5 | 214.5 | 208.8 | 201.4 | 200.9 | 193.2 |

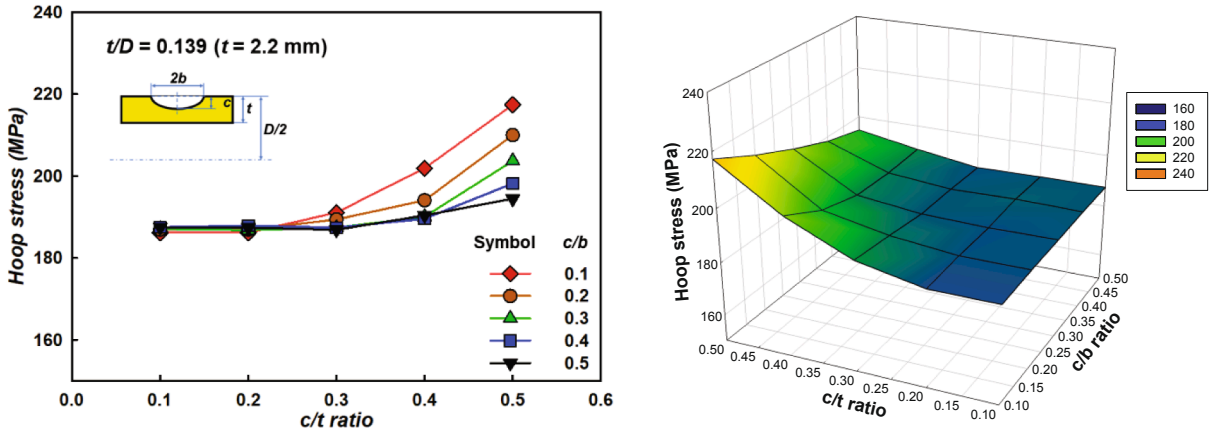


(a)

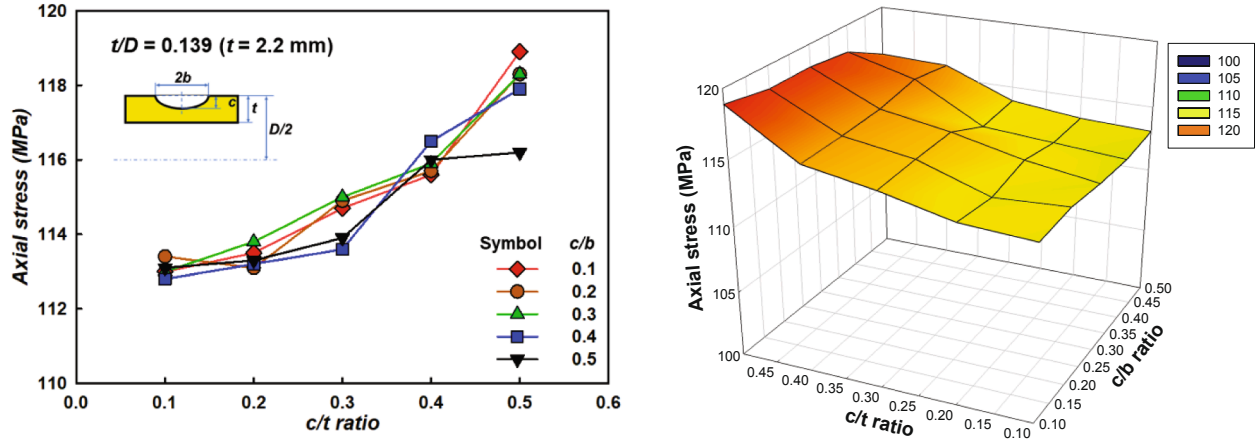


(b)

**Fig. 4.** FEA results for hoop and axial stress for different $c/t$ and $c/b$ ratios.

$$\sigma_z = \left\{ \frac{P_i r_i^2 - P_o r_o^2}{r_o^2 - r_i^2} + \frac{E\alpha(T_o^* - T_i^*)}{2(1-\nu^2)\ln(r_o/r_i)} \left[ \frac{2r_o^2}{r_o^2 - r_i^2} \ln\left(\frac{r_o}{r_i}\right) - 1 \right] \right\} \times F_{e,z} \left(\frac{c}{t}, \frac{c}{b}\right), \tag{16}$$

where $F_{e,z}$ is the axial stress correction function for local thinning, which depends on $c/t$ (0.1−0.5) and $c/b$ (0.1−0.5). $F_{e,z}$ is given by Eq. (17):

$$F_{e,z}\left(\frac{c}{t}, \frac{c}{b}\right) = \frac{\sigma_{z\_FEM}}{\frac{P_i r_i^2 - P_o r_o^2}{r_o^2 - r_i^2} + \frac{E\alpha(T_o^* - T_i^*)}{2(1-\nu^2)\ln(r_o/r_i)} \left[ \frac{2r_o^2}{r_o^2 - r_i^2} \ln\left(\frac{r_o}{r_i}\right) - 1 \right]} \tag{17}$$

After repeating the steps outlined in Section 3.2.1, the response values ($F_{e,z}$) are also listed in Table 3. The correction function $F_{e,z}$ was obtained using Eq. (18):

$$F_{e,z}\left(\frac{c}{t}, \frac{c}{b}\right) = 1.1563 - 0.0213\left(\frac{c}{t}\right) + 0.0473\left(\frac{c}{b}\right) + 0.2843\left(\frac{c}{t}\right)^2 - 0.0657\left(\frac{c}{b}\right)^2 - 0.0810\left(\frac{c}{t}\right)\left(\frac{c}{b}\right) \tag{18}$$

The resulting $R^2$ and $R^2_{\text{adjusted}}$ values for $F_e$ and $F_{e,z}$ are listed in Table 4.

Since the purpose of this paper is to suggest approximate stress estimation equations when a local thinning exists on the outside of the tube, the case of no thinning is not included in this equation. The Egs. (15) and (18) are useful in the presence of a local wall-thinning of the ranges of $c/t$ = 0.1–0.5 and $c/b$ = 0.1–0.5. Even though the case of no defect or negligible size of local thinning defect is not considered in the proposed equations that would not deteriorate the usefulness of the proposed equations. Including the non-defect point of $c/t$ = 0 in the proposed equations will considerably deteriorate the accuracy of the stress equations in the range of practical use (0.1-0.5 of c/t).

## 4. Results and discussion

### 4.1. Comparison of FE simulation results with the proposed equations

Analysis of variance (ANOVA) is used to compare the results of $F_e$ and $F_{e,z}$ equations with the RSM method above. The ANOVA results for the correction functions $F_e$ and $F_{e,z}$ are presented in Table 5. Similar

**Table 3**
Sample data and the corresponding response values $F_e$ and $F_{e,z}$.

| Model Number | Design variable | | Response | |
|---|---|---|---|---|
| | $c/t$ ratio | $c/b$ ratio | $F_e$ | $F_{e,z}$ |
| 1 | 0.1 | 0.1 | 1.145 | 1.163 |
| 2 | 0.2 | 0.1 | 1.145 | 1.166 |
| 3 | 0.3 | 0.1 | 1.175 | 1.178 |
| 4 | 0.4 | 0.1 | 1.242 | 1.188 |
| 5 | 0.5 | 0.1 | 1.337 | 1.221 |
| 6 | 0.1 | 0.2 | 1.150 | 1.165 |
| 7 | 0.2 | 0.2 | 1.150 | 1.162 |
| 8 | 0.3 | 0.2 | 1.165 | 1.180 |
| 9 | 0.4 | 0.2 | 1.194 | 1.189 |
| 10 | 0.5 | 0.2 | 1.292 | 1.215 |
| 11 | 0.1 | 0.3 | 1.151 | 1.161 |
| 12 | 0.2 | 0.3 | 1.149 | 1.169 |
| 13 | 0.3 | 0.3 | 1.153 | 1.181 |
| 14 | 0.4 | 0.3 | 1.169 | 1.191 |
| 15 | 0.5 | 0.3 | 1.253 | 1.215 |
| 16 | 0.1 | 0.4 | 1.153 | 1.159 |
| 17 | 0.2 | 0.4 | 1.156 | 1.163 |
| 18 | 0.3 | 0.4 | 1.153 | 1.167 |
| 19 | 0.4 | 0.4 | 1.166 | 1.197 |
| 20 | 0.5 | 0.4 | 1.219 | 1.211 |
| 21 | 0.1 | 0.5 | 1.153 | 1.162 |
| 22 | 0.2 | 0.5 | 1.153 | 1.164 |
| 23 | 0.3 | 0.5 | 1.150 | 1.170 |
| 24 | 0.4 | 0.5 | 1.171 | 1.192 |
| 25 | 0.5 | 0.5 | 1.196 | 1.194 |

**Table 4**
Error diagnostics for the response values $F_e$ and $F_{e,z}$.

| Measure | RSM method | | ANOVA method | |
|---|---|---|---|---|
| | Response | | Response | |
| | $F_e$ | $F_{e,z}$ | $F_e$ | $F_{e,z}$ |
| $R^2$ | 0.9551 | 0.9496 | 0.9552 | 0.9496 |
| $R^2_{adjusted}$ | 0.9433 | 0.9365 | 0.9434 | 0.9363 |

**Table 5**
ANOVA results for the effects of tube dimensions.

| Source | $F_e$ | | $F_{e,z}$ | |
|---|---|---|---|---|
| | F-Value | P-value | F-Value | P-value |
| $c/t$ | 231.03 | 0 | 324.6 | 0 |
| $c/b$ | 42.10 | 0 | 5.59 | 0.029 |
| $c/t$ *$c/t$ | 66.35 | 0 | 23.51 | 0 |
| $c/b$ *$c/b$ | 3.49 | 0.077 | 1.26 | 0.276 |
| $c/t$ *$c/b$ | 62.40 | 0 | 2.73 | 0.115 |

regression equations are produced for both methods, and the $c/t$ ratio is the most important variable in the regression equations. This conclusion is in accordance with the FEA results presented in Section 2.2. Fig. 5 compares the FE simulation results with the proposed equations for $F_e$ and $F_{e,z}$. The results derived from the proposed equations agree with the FE simulation results, with an average difference of only 5%.

A comparison of the hoop stress and axial stress results from FEA and the proposed equations are presented in Figs. 6 and 7, respectively. The results calculated from Eqs. (10) and (16) are a close fit to the FEA results. The difference in hoop stress and axial stress between the two methods is insignificant.

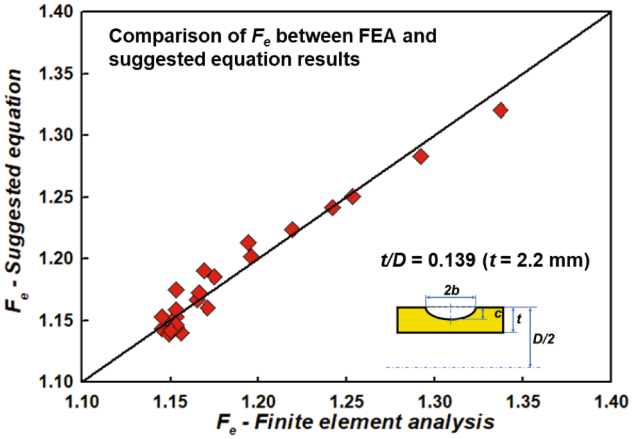


(a)

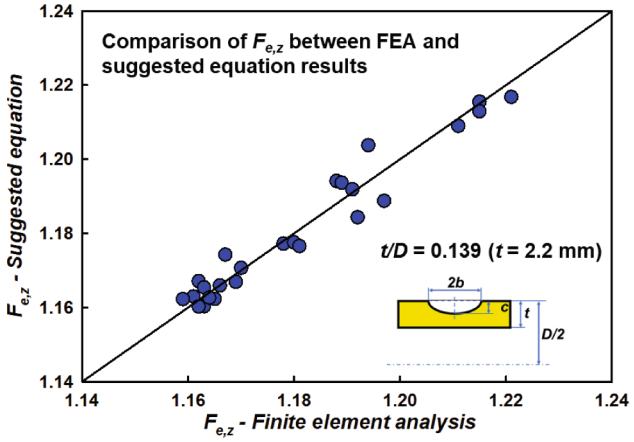


(b)

**Fig. 5.** Comparison of FE simulation results with the proposed equations: (a) $F_e$ correction function and (b) $F_{e,z}$ correction function.

In this study, the wall thickness and outer diameter of the tube are constant ($t/D = 0.139$ and $t = 2.2$ mm). In order to study the effect of the longitudinal length of the local wall-thinning defect ($2b$) on stress, a fixed value of $c/t = 0.1$ is employed (Table 6). The three forms of stress do not exhibit any significant change as the defect length increased (or the $c/b$ ratio decreased from 0.5 to 0.1).

In order to study the effect of depth (via the $c/t$ ratio) on the stresses for a tube with a local wall-thinning defect, a fixed value of $c/b = 0.1$ is employed (Table 7). The results show that the stresses increased when the $c/t$ ratio increased. The discrepancy in the stresses between the FEA results and those calculated using the analytic equations is lower than 5%.

Thus, it is clear that the defect depth ($c$) is the main factor influencing the stresses (hoop, axial, and von Mises stress) affecting a tube with a local wall-thinning defect. The length of the defect ($2b$) also has an effect on the hoop and axial stress. When the depth increased ($c/t = 0.3$–$0.5$), the effect of $b$ was most obvious.

### 4.2. Plugging criteria for a tube with a local wall-thinning defect

Determining the plugging criteria for a tube with a local wall-thinning defect requires the maximum depth ($c$) and longitudinal length ($2b$) at which the tube is destroyed to be calculated. The plugging

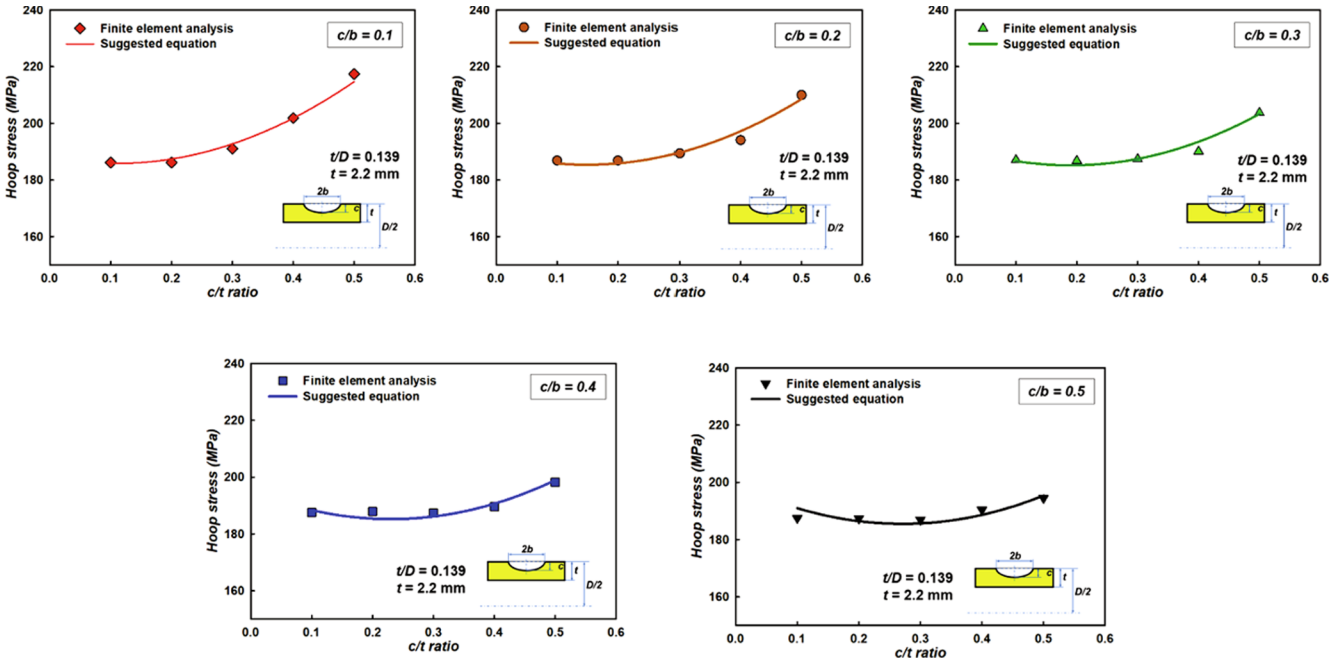


**Fig. 6.** Comparison of hoop stress between FEA and the proposed equation.

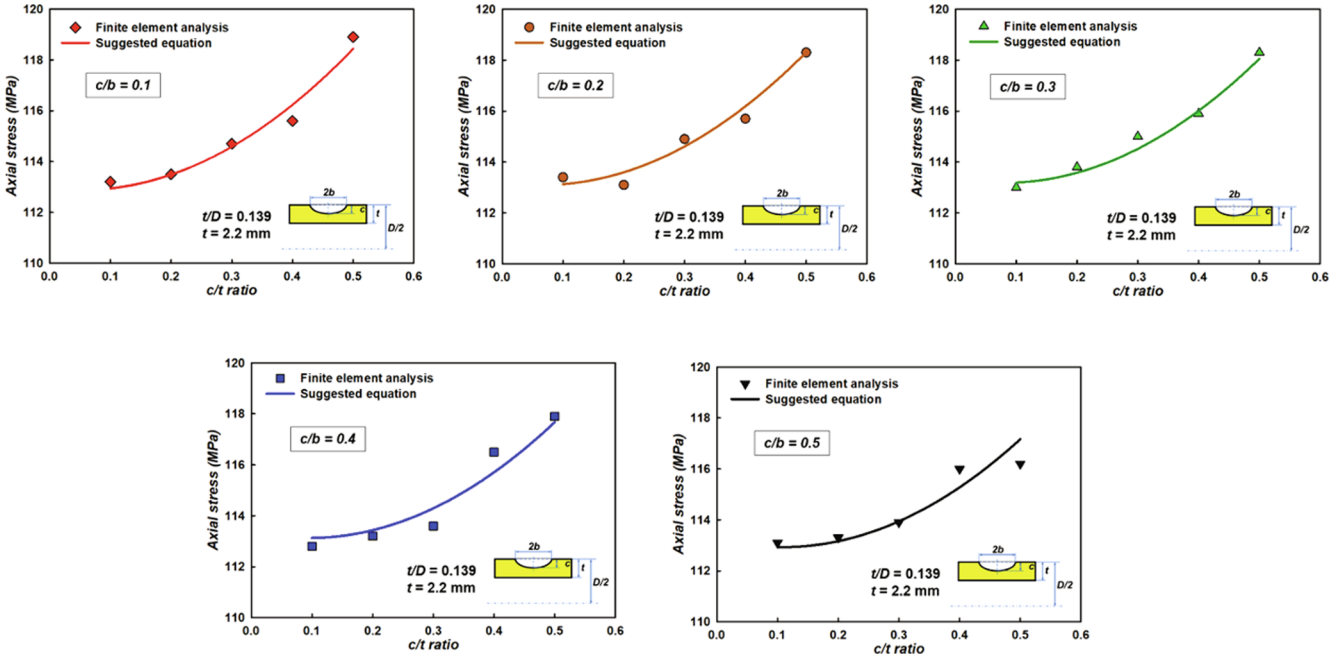


**Fig. 7.** Comparison of axial stress between FEA and the proposed equation.

**Table 6**
Comparison of the calculated stresses and FEA results at $c/t = 0.1$.

| $c/b$ ratio | Von Mises stress | | | Hoop stress | | | Axial stress | | |
|---|---|---|---|---|---|---|---|---|---|
| | FEA (MPa) | Calculated (MPa) | Discrepancy (%) | FEA (MPa) | Calculated MPa) | Discrepancy (%) | FEA (MPa) | Calculated (MPa) | Discrepancy (%) |
| 0.1 | 190.4 | 195.8 | 2.84 | 186.2 | 185.9 | −0.16 | 113.2 | 112.9 | −0.27 |
| 0.2 | 193.5 | 195.8 | 1.19 | 186.9 | 185.8 | −0.59 | 113.4 | 113.1 | −0.26 |
| 0.3 | 193.1 | 196.4 | 1.71 | 187.1 | 186.7 | −0.21 | 113.0 | 113.2 | 0.18 |
| 0.4 | 193.1 | 197.7 | 2.38 | 187.5 | 188.4 | 0.48 | 112.8 | 113.1 | 0.27 |
| 0.5 | 194.5 | 199.6 | 2.62 | 187.5 | 191.0 | 1.87 | 113.1 | 112.9 | −0.18 |

**Table 7**
Comparison of the calculated stresses and FEA results at $c/b = 0.1$.

| $c/t$ ratio | Von Mises stress | | | Hoop stress | | | Axial stress | | |
|---|---|---|---|---|---|---|---|---|---|
| | FEA (MPa) | Calculated (MPa) | Discrepancies (%) | FEA (MPa) | Calculated (MPa) | Discrepancies (%) | FEA (MPa) | Calculated (MPa) | Discrepancies (%) |
| 0.1 | 190.4 | 195.8 | 2.81 | 186.2 | 185.9 | −0.18 | 113.2 | 112.9 | −0.23 |
| 0.2 | 190.6 | 197.0 | 3.38 | 186.2 | 187.4 | 0.66 | 113.5 | 113.5 | 0 |
| 0.3 | 194.5 | 201.3 | 3.49 | 191.1 | 192.8 | 0.87 | 114.7 | 114.6 | −0.09 |
| 0.4 | 201.0 | 208.6 | 3.76 | 201.9 | 201.9 | 0 | 115.6 | 116.2 | 0.55 |
| 0.5 | 214.5 | 219.0 | 2.08 | 217.4 | 214.7 | −1.23 | 118.9 | 118.4 | −0.38 |

criteria are calculated using von Mises stress theory considering the safety factor ($n = 1.5$), as shown in Eq. (19) (HEI, 2010; ASME boiler and pressure vessel code, Section I; ASME boiler and pressure vessel code, Section VIII; Ling, 2000; API, 2007):

$$\sigma_{Von} \leqslant \sigma_{allow} = \frac{\sigma_{proof}}{n} = \frac{(\sigma_{YS} + \sigma_{UTS})/2}{n}, \tag{19}$$

where $\sigma_{proof}$ is the proof stress, the average stress of the yield strength and the ultimate tensile strength of the material. Choice of 1.5 as a safety factor and the proof stress as an allowable design stress are used in this study. But, the choice of the allowable stress in combination with the safety factor depends on the manufacturer or the regulator of the feedwater heater. In the most of the referred codes such as ASME (ASME boiler and pressure vessel code, Section I; ASME boiler and pressure vessel code, Section VIII), API (2007), and HEI (2013), the allowable stress is defined differently. Von Mises stress is calculated based on the hoop stress from Eq. (10), the axial stress from Eq. (16), and the radial stress (constant value, −35.89 MPa).

Based on the numerical solution, the plugging criteria for a tube with a local wall-thinning defect is determined to be $c_{max} = 1.03$ mm ($c/t = 0.468$) and $b_{max} = 10.3$ mm ($c/b = 0.1$). When the tube with a local wall-thinning defect reaches these values, the tube should be plugged or replaced.

A plugging criteria for a local wall-thinning geometry with finite length in tube axial direction, is suggested in this study. Consideration of the tube axial dimension of the thinned area, not assuming it as infinite, makes the problem complex. But it can give more realistic plugging criteria. Further studies are required for various local thinning models with different types of local thinning shape of finite size. There are some particular shapes of local thinning in nuclear and fossil power plants for industrial application. Also experimental verification of the suggested plugging criteria need to be conducted, based on a well-planned experimental program or using the existing experimental data.

## 5. Conclusions

The determination of the plugging criteria and stresses on the inner surface of a tube with a local wall-thinning defect was assessed based on regression methods in the present study. A feedwater heater tube with typical local wall-thinning defects was analyzed using finite element analysis. The following conclusions were drawn:

- Analytic equations for the stresses (hoop and axial stress) on the inner surface of a tube with a local wall-thinning defect are proposed.
- The plugging criteria for a tube with a local wall-thinning defect are determined to be $c_{max} = 1.03$ mm ($c/t = 0.468$) and $b_{max} = 10.3$ mm ($c/b = 0.1$) using von Mises stress theory. When the tube reaches these values, it should be plugged or replaced.
- Maximum stress occurs on the inner surface of the tube. The radial stress on the inner surface does not depend on the $c/t$ or $c/b$ ratio.
- Depth ($c$) is the main factor influencing the stresses (hoop, axial, and von Mises stress) for a tube with a local wall-thinning defect. Hoop and axial stresses increase as the depth increases.
- The longitudinal length ($2b$) also has an effect on the hoop and axial stress. When the depth increases ($c/t = 0.3$−$0.5$), the effect of $b$ is most obvious.
- This suggested process is independent of the material properties and operating conditions (i.e., pressure and thermal loads), and it can be applied to other tube materials under various operating conditions in high-pressure feedwater heaters if the pressure and temperature fluctuate within a small range.

## Acknowledgements

This work was supported by the Korea Institute of Energy Technology Evaluation and Planning (KETEP) and the Ministry of Trade, Industry & Energy (MOTIE) of the Republic of Korea (No. 20141010101850).

Hong Bo Dinh: conducting FEA, original draft writing, revising the paper and editing, Kee Bong Yoon: project planning, conceptualization, methodology determination, funding acquisition, project administration, reviewing the draft paper, supervising.

## References

API 579-1/ASME FFS-1: Fitness-for-service, API, The American Society of Mechanical Engineers, 2007.
ASME boiler and pressure vessel code, Section I: Rules for construction of power boilers, American Society of Mechanical Engineers, 2010.
ASME Boiler and Pressure Vessel Code, Section II, Part D: Properties, American Society of Mechanical Engineers, 2013.
ASME boiler and pressure vessel code, Section VIII, Division 1: Rules for construction of pressure vessels, American Society of Mechanical Engineers, 2010.
Chen, Z., Zhu, W., Di, Q., Wang, W., 2015a. Burst pressure analysis of pipes with geometric eccentricity and small thickness-to-diameter ratio. J. Petrol. Sci. Eng. 127, 452–458.
Chen, Z., Zhu, W., Di, Q., Wang, W., 2015b. Prediction of burst pressure of pipes with geometric eccentricity. J. Pressure Vessel Technol. 137 (6), 061201.
Chen, Z., Zhu, W., Di, Q., Li, S., 2016. Numerical and theoretical analysis of burst pressures for casings with eccentric wear. J. Petrol. Sci. Eng. 145, 585–591.
Dinh, H.B., Yu, J.M., Yoon, K.B., Park, C., Ryu, S.W., 2018. Plugging criteria for thinned high-pressure feedwater heater tubes considering pressure and thermal loading. J. Mech. Sci. Technol. 32 (12), 5637–5645.
Eslami, M.R., Hetnarski, R.B., Ignaczak, J., Noda, N., Sumi, N., Tanigawa, Y., 2013. Theory of Elasticity and Thermal Stresses, vol. 197 Springer, Dordrecht.
Standards for shell and tube heat exchangers, Heat Exchanger Institute Inc., Fifth Ed., Ohio USA, 2013.
Hui, H., Li, P., 2010. Plastic limit load analysis for steam generator tubes with local wall-thinning. Nucl. Eng. Des. 240, 2512–2520.
Kanlıkama, B., Abuşoğlu, A., Güzelbey, I.H., 2013. Coupled thermoelastic analysis of thick-walled pressurized cylinders. Int. J. Energy Power Eng. 2 (2), 60–68.
Kim, J.S., Lee, M.W., Kim, Y.J., Kim, J.W., 2019. Numerical validation of burst pressure estimation equations for steam generator tubes with multiple axial surface cracks. Nucl. Eng. Technol. 51, 579–587.
Ling, J., 2000. The evolution of the ASME boiler and pressure vessel code. J. Pressure Vessel Technol. 122 (3), 242–246.
Moreira Junior, N.M., Carrasquila, A.A., Figueiredo, A., da Fonseca, C.E., 2015. Worn pipes collapse strength: experimental and numerical study. J. Petrol. Sci. Eng. 133, 328–334.
Poworoznek, P.P., 2008. Elastic-plastic behavior of a cylinder subject to mechanical and

thermal loads, M.Sc. thesis, Rensselaer Polytechnic Institute, Hartford, CT.
Simpson, T.W., Mistree, F., 2001. Kriging models for global approximation in simulation-based multidisciplinary design optimization. AIAA J. 39 (12), 2233–2241.
Tun, N.N., Yang, H.S., Yu, J.M., Yoon, K.B., 2016. Creep crack growth analysis using $C_t$-parameter for internal circumferential and external axial surface cracks in a pressurized cylinder. J. Mech. Sci. Technol. 30 (12), 5447–5458.
Wang, T., Yan, X., Wang, J., Yang, X., Jiang, T., Huang, H., 2013. Investigation of the ultimate residual strengthen of a worn casing by using the arc-length algorithm. Eng. Fail. Anal. 28, 1–15.
Yoon, K.B., Park, T.G., Saxena, A., 2003. Creep crack growth analysis of elliptic surface cracks in pressure vessels. Int. J. Press. Vessels Pip. 80 (7–8), 465–479.
Zhang, Q., Lian, Z., Lin, T., Deng, Z., Xu, D., Gan, Q., 2016. Casing wear analysis helps verify the feasibility of gas drilling in directional wells. J. Nat. Gas Sci. Eng. 35, 291–298.